Shock temperatures and melting curve of an Fe–Ni–Cr alloy up to 304 GPa

HPSTAR
1371-2022

View Online   Export Citation   CrossMark

Bo Gan,[1] Jun Li,[2] Qiang Wu,[2] Gang Jiang,[1] Hua Y. Geng,[2] Ye Tan,[2] Xianming Zhou,[2]
Toshimori Sekine,[3] Zhipeng Gao,[2,a] and Youjun Zhang[1,4,a]

AFFILIATIONS

[1]Institute of Atomic and Molecular Physics, Sichuan University, Chengdu 610065, China
[2]National Key Laboratory for Shock Wave and Detonation Physics, Institute of Fluid Physics, CAEP, Mianyang 621900, China
[3]Center for High Pressure Science and Technology Advanced Research, Shanghai 210203, China
[4]Key Laboratory of High Energy Density Physics and Technology of Ministry of Education, Sichuan University, Chengdu 610065, China

Note: This paper is part of the Special Topic on Shock Behavior of Materials.
[a]**Authors to whom correspondence should be addressed:** zhangyoujun@scu.edu.cn and z.p.gao@foxmail.com

ABSTRACT

The melting temperatures of Fe–Ni alloys and their densities in the liquid state at relevant pressure–temperature (P–T) conditions present in the core are of great importance for understanding the composition and thermal structure of the Earth's core. We measured shock temperatures of the Fe–11Ni–18Cr (wt. %) alloy up to ~304 GPa using a special target configuration, a quasi-spectral pyrometer, and velocimeter diagnostics in a two-stage light-gas gun. The present results show that Fe–11Ni–18Cr starts to melt at the pressure of 210 (8) GPa and 4700 (300) K and completes at the pressure of 280 (10) GPa and 5250 (350) K under shock loading, which is ~1000 K lower than some previous shock temperature measurements. The melting temperatures of the Fe–11Ni–18Cr alloy are 4100 (250) K and 5500 (450) K at the pressures present at the core-mantle boundary (~136 GPa) and inner-core boundary (~330 GPa), respectively, which are slightly lower than that of pure iron. Combined with the previous results of the pressure–density measurements at Hugoniot states, our results indicate that the presence of limited amounts of Ni and Cr into Fe has a minor effect on its melting curve and density in the liquid state, suggesting that sufficient light elements are required in the outer core to satisfy both the core density deficit and the reduced melting temperature.

I. INTRODUCTION

The liquid outer core solidifies at the inner-core boundary (ICB, ~330 GPa), where the upper limit of the ICB temperature can be anchored by the melting points of iron (Fe) and its alloys at ~330 GPa.[1] The melting curves of iron and iron alloys have been widely investigated through high P–T experiments and theoretical simulations.[1–9] Some recent shock and static diamond anvil cell (DAC) experiments obtained a consensus melting curve of iron up to ~260 GPa, indicating a melting temperature of ~6000–6400 K at the ICB pressure.[1,4–6] Possible additional components in the core, including Ni, light elements, and trace elements [such as chromium (Cr)],[10,11] are expected to have a significant influence on the physical properties of iron, including the crystal structure, seismic velocity, density, and melting behavior.[12–17] The contributions of Ni, light element(s), and trace element(s) to the density of the outer core (as the core density deficit, cdd) depend on thermal EoSs of the liquid iron and iron alloys.[18,19] The cdd plays an indispensable role in the geochemical models of the core composition.[18] However, creating the relevant P–T conditions present in the core and measuring the liquid density is quite challenging in the static compression experiments.[20,21] The pressure-temperature-density (P–T–ρ) relation of liquid iron was still limited up to 116 GPa and 4350 K in a recent laser-heated DAC study, which reported that the cdd was constant at 7.5%–7.6%.[21] Shock compression experiments have identified the pressure–density (P–ρ) relations of liquid iron and iron alloys (such as Fe–Ni and Fe–Ni–Cr alloys) up to the ICB pressure along the principal Hugoniot,[22–24] while the exact Hugoniot temperatures were not well constrained in the previous experiments.[25–27]

A Ni content of 5%–10% is commonly assumed in the Earth's core, and Cr is an important trace siderophile element. High-precision measurements of Cr stable isotopes in meteorites indicated that Cr could have been partitioned into Earth's core under conditions prevailing in the lower mantle or at the base of a magma ocean.[28–32] Based on a mass balance between chondrites and the bulk Earth, the core is likely to contain a major fraction (60%–65%) of the Earth's Cr budget,[11,33] and the abundance of Cr in the core is estimated to be ~1 wt. %.[11] Therefore, it is essential to determine the effects of Ni and Cr on the physical properties of Fe under the relevant P–T conditions of the core and to understand the origin, evolution, and current states of the Earth's core.

Recent laser-heated DAC experiments coupled with *in situ* Synchrotron Mössbauer Spectroscopy (SMS) or x-ray absorption spectroscopy (XAS) indicated that the melting temperatures of Fe–Ni alloys with 10–20 wt. % of nickel were 200–400 K lower than that of pure Fe at a pressure near the core-mantle boundary (CMB, ~136 GPa).[34,35] At higher pressures, the melting temperature of an Fe–9Ni–19Cr (wt. %) film (12–14 μm thick) measured by a four-channel optical pyrometry[27,36] was 1000–2000 K lower than that of an Fe film in shock-wave compression experiments with the same setup,[25,26] indicating that the addition of Ni and/or Cr caused a significant melting temperature depression in Fe. However, a recent shock experiment using a quasi-spectral pyrometer and optimized sample assemblages has determined the melting temperature of iron up to ~256 GPa,[1] which was 1000–2000 K lower than the measurements of previous shock experiments,[25,26] but was overall consistent with the results of the *ab initio* computations[3,37] and laser-heated DAC experiments.[4,5] These results indicate that the melting temperature of the Fe–9Ni–19Cr film may suffer anomalously high temperatures due to the following two aspects: (a) tiny gaps between sample and window and (b) low measurement accuracy of the pyrometer. Thus, the new measurement encourages us to investigate the shock melting curve of the Fe–Ni–Cr alloy and to develop thermal EoS of the liquid Fe–Ni–Cr at the relevant P–T conditions of the outer core.

In this study, we measured the temperatures of an Fe–11 wt. % Ni–18 wt. % Cr alloy (hereafter Fe–11Ni–18Cr) up to ~304 GPa by a two-stage light-gas gun. The accuracy of the measured temperature was ensured by improving the resolution of the pyrometer (4–6 vs 16 channels in the wavelength of 300–800 nm) and the processing of the sample target (film vs dense sample with an ideal interface treatment). Our results are ~1000 K lower than some previous shock temperature measurements.[27,36] The melting temperatures of the Fe–11Ni–18Cr alloy were obtained from Hugoniot temperature measurements at the solid–liquid phase boundary and were estimated to be 4100 (250) and 5500 (450) K at pressures of CMB and ICB, respectively. We suggest that the integration of the limited amounts of Ni and Cr into Fe has a minor effect on the melting temperature and liquid density under Earth's core conditions. Our study further constrains the temperature at the ICB and the core's composition.

II. EXPERIMENTS

A. Materials

A homogeneous Fe–11Ni–18Cr alloy was used as the starting sample. The sample density was 7.90 (0.01) g/cm³ as determined by

TABLE I. Chemical composition of the Fe–Ni–Cr samples.

Elements (wt. %)	This study	Duffy and Ahrens[38]	Bass *et al.*[27]	McQueen *et al.*[39]
Fe	68	69.7	69.3	68
Cr	18	19.3	19.4	19
Ni	11	8.2	9.1	10
Mn	2	1.3	…	2
Si	<1	0.4	0.7	1
Total	>99	98.9	98.5	100
Density (g/cm³)	7.90 (0.01)	7.88 (0.01)	7.82 (0.08)	7.896

the Archimedean method. The initial density and chemical composition of our sample were nearly the same as those of the Fe–Ni–Cr samples used for the previous shock temperature and Hugoniot sound-velocity measurements, which contained ~8–11 wt. % Ni and ~18–19 wt. % Cr (Table I).[27,38,39] Our sample was machined into a 3.0-mm-thick disk with a diameter of 40 mm. A single-crystal lithium fluoride (LiF) with [100] orientation was used as the window, which has a diameter of ~23 mm and a thickness of ~8 mm. In the previous work, a vapor-deposited film (12–14 μm thick) was used to minimize the surface roughness; however, the recorded voltage profiles showed that the sample–window interface still suffered from a more complex thermal interaction than the theoretical model,[27,36] and the possible porosity could have been introduced during deposition.[40,41] The effect of a gap of ~1 μm on the temperature measurement by the spectro-radiometric method has been discussed by Urtiew and Grover.[40,41] When the shock wave arrives at the gap, which can be treated as a free surface of the sample, the shocked material will release to an ambient pressure and an elevated temperature. The hot material subsequently impacts the surface of the window. Consequently, the sample will be reshocked to a higher temperature, which is significantly larger than the initial Hugoniot temperature. In this study, thick samples were employed and their surfaces were optically polished to a mirror finish to achieve near-ideal contact. More details can be found in a recent study.[1]

B. Experimental methods

Shock wave experiments were conducted by a 30-mm-bore two-stage light-gas gun at the Institute of Fluid Physics, China. The experimental setup for shock temperature measurement is shown in Fig. 1. Tantalum (Ta) and copper (Cu) were used as flyer plates, which had a diameter of ~23 mm and a thickness of ~2 mm. The impact velocity of the flyer was measured using the optic beam break-out (OBB) method within ~1% uncertainty. We used an optical pyrometer with 16 channels to measure the shock temperatures and employed a photon Doppler velocity interferometer (PDV) to measure the particle velocity profiles at the Fe alloy/LiF interface simultaneously. Black epoxy glue was coated on the curved surface of the cylinder window, ensuring that the interface was clamped inside the target box. The interior of the target box was evacuated to less than ~1 Pa before the shot to eliminate possible strong scattering of the emitted light. More experimental details can be seen in the previous studies.[1,42]
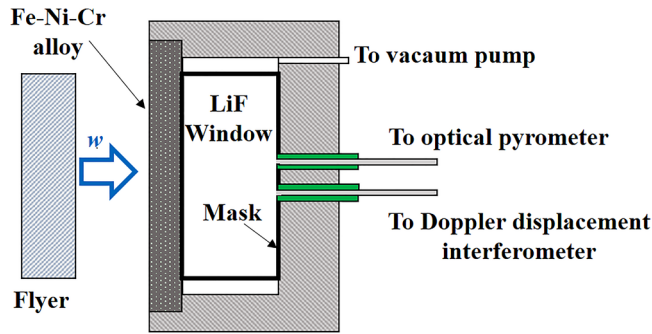
FIG. 1. Schematic diagram of the experimental setup for simultaneously measuring the interface temperature and particle velocity. w represents the impact velocity of the flyer, which was measured by the optic beam break-out (OBB) method. We used the optical pyrometer and photon Doppler velocity interferometer to measure the interface temperature and particle velocity, simultaneously. The interior of the target box was evacuated to be less than ~1 Pa before the shot.

Five plate impact experiments were performed to measure the interfacial temperatures and particle velocity profiles at the Fe alloy/LiF interface. The impact velocity ranges from 4.78 to 7.03 km/s, where the Hugoniot pressure (P_H) is calculated by the impedance matching method[43–45] based on the measured impact velocities of the flyer and the known Hugoniot relations of the Fe alloy,[38] Cu,[46,47] and Ta[48] (Table II). The measured particle velocities were used to determine the interface pressure (P_R) using the Hugoniot relation of the LiF.[49] The uncertainties of P_H and P_R were obtained using the methods for error analysis in previous shock compression studies.[46,50] The impact conditions and results of the Hugoniot states of the Fe–11Ni–18Cr alloy are listed in Table II.

A typical spectral radiance history at the Fe alloy/LiF interface in the measurements is shown in Fig. 2. The uncertainty of the measured spectral radiance is ~2%.[51] The spectral radiance sharply increased at point A, indicating the arrival of shock waves at the interface. The spectral radiance from A to B remained nearly

constant at all pyrometer wavelengths during shock compression, indicating that our special target configuration avoids strong thermal emission. The spectral radiance started to decrease with the arrival of the rarefaction wave at point B. Temperature (T_I) and emissivity (ε) at the interface were obtained by fitting the measured spectral intensities to Planck's equation for gray-body radiation (Fig. 3).[1,42] We estimated the uncertainties of T_I and ε using the method of Ref. 52. The present pyrometer has a time resolution of ~3 ns, which allows us to obtain the time-resolved temperature profile at the interface (Fig. 4).

The particle velocity profiles at the interface between the sample and the LiF window show a clear plastic single-wave structure (Fig. 4), as measured using the PDV during the pyrometer measurements simultaneously. Both the interfacial temperature and the particle velocity profile exhibit a stable plateau (~530 ns) between points A and B (Fig. 4). Therefore, the interface reached physically thermal equilibrium during the present measurements.[1,42]

III. RESULTS AND DISCUSSION

A. Shock temperature of Fe–11Ni–18Cr alloy

The shock impedance of LiF is lower than that of the Fe–11Ni–18Cr alloy.[38,49] Consequently, the Hugoniot pressure (P_H) is partially released to the interface pressure (P_R) when the shock wave propagates from the sample to the LiF window. The partial release at the interface will be treated as a quasi-isentropic process.[53] Thus, the Hugoniot temperature (T_H) of the Fe–11Ni–18Cr alloy could be derived from the release temperature (T_R) at P_R according to the Mie–Grüneisen thermal equation,[1]

$$T_H = T_R \exp\left[-\int_{V_R}^{V_H} (\gamma/V)\, dV\right], \qquad (1)$$

where V_H and V_R are the volumes of the Fe–11Ni–18Cr alloy at the pressures of P_H and P_R, respectively, and γ is the Grüneisen parameter, which can be taken from previous shock experiments.[38] Based on the one-dimensional thermal conduction model,[54] T_R is calculated from the measured temperature T_I as follows:

TABLE II. Impact conditions and the Hugoniot and partially released states of Fe–11Ni–18Cr alloy in the pyrometer experiments. Notes: w is the measured impact velocity and its uncertainty is estimated to be 1 % at the 2σ level; u_{pi} is the measured particle velocity at the Fe–11Ni–18Cr alloy/LiF interface and its uncertainty is given at the 2σ level, including the inherent accuracy of the PDV measurement and uncertainties due to the fluctuation of particle velocity profiles; u_p, U_S, and P_H are the particle velocity, shock-wave velocity, and Hugoniot pressure, respectively, and are calculated from w and the known Hugoniot relations of the flyers and Fe–Ni–Cr alloy; and P_R is the interface pressure calculated from u_{pi} and the Hugoniot relation of LiF. The Hugoniot parameters used in this study are U_s (km/s) = 4.58 (0.01) + 1.49 (0.01)u_p with a density of 7.87 (0.02) g/cm^3 for the Fe–11Ni–18Cr alloy;[38] U_s (km/s) = 3.310 (0.008) + 1.296 (0.005)u_p with a density of 16.684 (0.03) g/cm^3 for flyer Ta;[48] U_s (km/s) = 3.933 (0.004) + 1.500 (0.025)u_p with a density of 8.939(5) g/cm^3 for flyer Cu;[46,47] and U_s (km/s) = 5.215 (0.02) + 1.351 (0.03)u_p with the density of 2.640 (0.002) g/cm^3 for LiF.[49] The uncertainties of u_p, U_S, P_H, and P_R are given at 2σ levels based on the methods for error analysis in previous shock compression studies.[46,50]

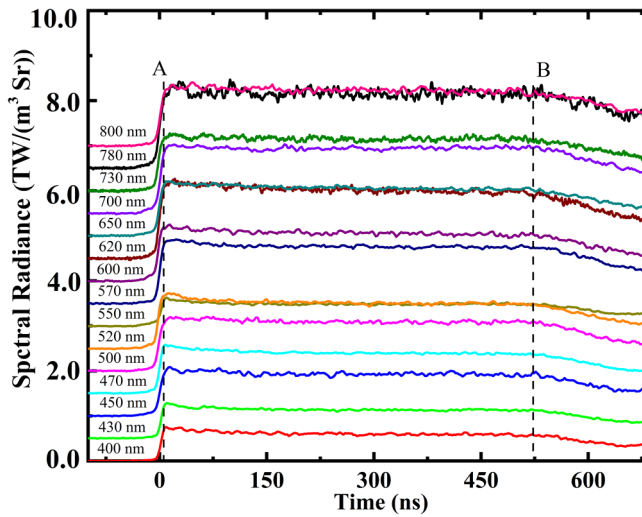| Shot No.	Flyer	w (km/s)	Sample/window u_p (km/s)	Sample u_p (km/s)	U_s (km/s)	P_H (GPa)	P_R (GPa)
ST-1	Ta	4.78 (0.05)	3.82 (0.04)	2.81 (0.02)	8.76 (0.04)	193.4 (2.9)	104.6 (1.7)
ST-2	Ta	5.21 (0.05)	4.15 (0.04)	3.05 (0.03)	9.13 (0.04)	219.5 (3.1)	118.6 (1.7)
ST-3	Ta	5.72 (0.06)	4.58 (0.05)	3.35 (0.03)	9.57 (0.05)	252.3 (4.0)	137.9 (2.3)
ST-4	Cu	7.03 (0.07)	4.88 (0.05)	3.59 (0.03)	9.92 (0.05)	280.1 (4.3)	152.1 (2.5)
ST-5	Ta	6.47 (0.06)	5.15 (0.05)	3.78 (0.04)	10.22 (0.05)	304.3 (4.4)	165.5 (3.0)

FIG. 2. Typical time-resolved spectral radiances at the interface of the Fe–11Ni–18Cr alloy/LiF window in shot No. ST-3. Point A represents the arrival time of shock waves at the sample/window interface, and point B indicates the arrival of rarefaction waves at the interface.

$$T_R = T_I + (T_I - T_W)/\alpha, \qquad (2)$$

where T_W is the shock temperature of the LiF window at P_R and α is the proportionality coefficient of the sample to the window, which can be calculated using the following equation:
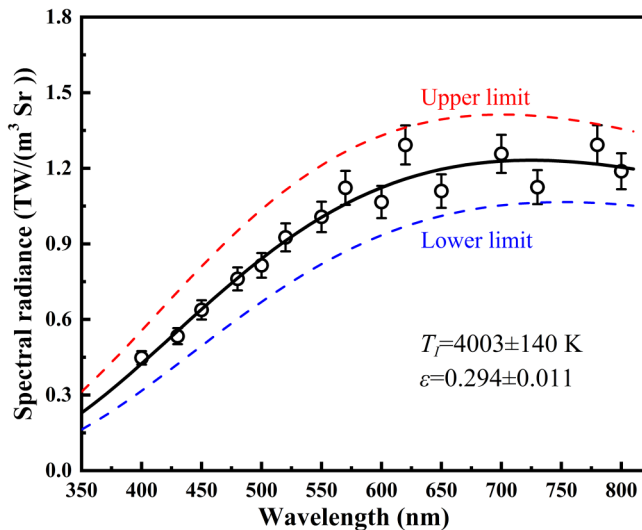

FIG. 3. Typical spectral radiances of the interface under shock loading as a function of wavelength in shot No. ST-3. The measured thermal radiances (open black circles) at discrete wavelengths are fitted to Planck gray-body spectrum (black lines) to derive the interface temperature and emissivity.
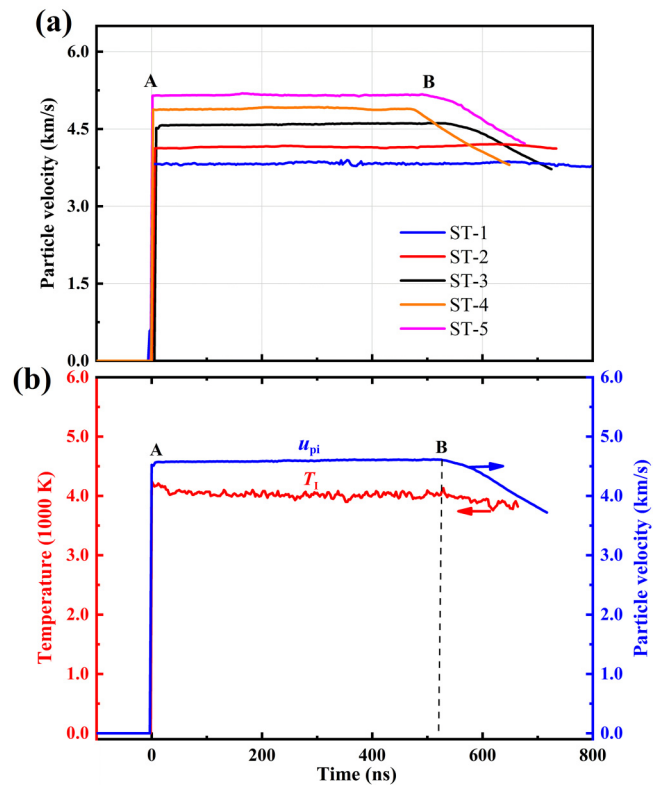

FIG. 4. Particle velocity profiles and interfacial temperature profile at the Fe–11Ni–18Cr alloy/LiF interface as a function of time. (a) Particle velocity profiles were measured by the PDV during the pyrometer measurements simultaneously. Particle velocity profiles show a clear plastic single-wave structure, and no elastic pioneer or phase-transition wave is observed. (b) A comparison of the typical profiles between the time-revolved particle velocity (u_{pi}) and interfacial temperature (T_I) in shot No. ST-3.

$$\alpha = \left[\frac{(\rho C \kappa)_S}{(\rho C \kappa)_W} \right]^{\frac{1}{2}}, \qquad (3)$$

where ρ, C, and κ are the density, heat capacity, and thermal conductivity, respectively, and the subscripts S and W denote sample and LiF window, respectively. The density and shock temperature values of the LiF window were obtained from previous experiments and calculations.[49,55] The heat capacity of the LiF window used in this study was ~1.638 J/g/K.[56] The thermal conductivity of the LiF window was taken from recent calculations and experiments.[49,57–59]

The heat capacity of the Fe–11Ni–18Cr alloy could be treated as a classical limit $C = 3R/M$ (where R is the gas constant and M is the molar mass). The thermal conductivity of the Fe–11Ni–18Cr alloy was considered equal to those of Fe and the Fe–10Ni alloy.[60–62] The coefficient α was calculated to be approximately 3.1–5.1, which was consistent overall with the value of 4.4 calculated by Bass *et al.*[27] The obtained values of T_H, T_R, and α in this

TABLE III. Melting and Hugoniot temperatures of the Fe–11Ni–18Cr alloy. Notes: T_I is the temperature of the Fe–11Ni–18Cr alloy/LiF interface obtained by fitting the measured spectral radiation intensities; the uncertainty of T_I is obtained by the sum of the pyrometric measurement error [including pyrometer calibration error, the photomultiplier tube (PMT) dynamic response error, and experimental measurement error] and the uncertainty on the determination of temperature using Planck's equation for gray-body radiation;[1] T_W is the temperature of the LiF window at the P_R and its uncertainty is roughly estimated from previous experiments and calculations;[49,55] κ_W is the thermal conductivity of the LiF window at the P_R and its uncertainty is obtained from previous experiments and calculations;[49,57–59] κ_S is the thermal conductivity of the sample at the P_R; α is the proportionality coefficient of the sample to the window calculated using Eq. (3); T_R is the temperatures of the Fe–11Ni–18Cr alloy at the partially released state (P_R) calculated from T_I; T_H is the temperature of the Fe–11Ni–18Cr alloy at Hugoniot state (P_H) calculated from T_R; and T_M is the melting temperature of the Fe–11Ni–18Cr alloy at P_R calculated from Eq. (6). The uncertainties are given in parameters at 2σ levels, and the uncertainties of T_H and T_M are derived from standard error propagations of the related parameters with errors.

Shot No.	T_I (K)	T_W (K)	κ_W at P_R (W/m/K)	κ_S at P_R (W/m/K)	α	T_R (K)	T_H (K)	T_M (K) at P_R
ST-1	3322 (201)	2235 (135)	4.9 (0.4)	70 (5)	3.1 (0.3)	3673 (242)	4373 (368)	…
ST-2	3722 (267)	2615 (140)	4.2 (0.4)	78 (5)	3.5 (0.4)	4038 (301)	4822 (458)	3880 (301)
ST-3	4003 (140)	3195 (160)	3.5 (0.4)	93 (5)	4.2 (0.5)	4195 (226)	5011 (252)	4099 (226)
ST-4	4198 (202)	3385 (170)	3.1 (0.4)	101 (10)	4.7 (0.5)	4371 (264)	5240 (337)	4284 (264)
ST-5	4583 (316)	3435 (175)	2.8 (0.4)	109 (10)	5.1 (0.5)	4808 (361)	5815 (449)	…

study are given in Table III. The obtained Hugoniot temperature of the Fe–11Ni–18Cr alloy in this study was ∼800–1300 K lower than that of the previous results (Fig. 5).[27,36]

We also calculated the Hugoniot temperature of the Fe–11Ni–18Cr alloy using a thermodynamic equation,[22,39]

$$dT = -T(\gamma/V)dV + \left(\frac{1}{2C_V}\right)[(V_0 - V)dP + (P - P_0)dV], \quad (4)$$

where γ/V was estimated to be a constant value of 17 according to the measured bulk wave velocities of the Fe–Ni–Cr alloy under shock loading.[38] The calculated solid Hugoniot temperature is ∼4294 K at ∼193 GPa (shot No. ST-1, Fig. 5), which is consistent with our obtained Hugoniot temperature by the pyrometer measurement (∼4373 K). The obtained Hugoniot temperature showed a discontinuity at a pressure of ∼219.5 GPa (shot No. ST-2, T_H = 4822 K) and was significantly lower than the calculated solid Hugoniot temperature (5228 K), indicating that the sample begins to melt.

B. Melting behaviors of Fe–11Ni–18Cr alloy at high pressures

Shock-induced superheating was proposed to reconcile the discrepancies of the melting temperatures of transition metals (e.g., iron, tantalum, and vanadium) at high pressures between the dynamic experiments[25,26,63,64] and static experiments.[3–5,37,65–69] Luo and Ahrens[70] proposed that the heating rate under shock compression is larger than that of the rearrangement of atoms needed for melting, suggesting that the shock-induced superheating would shift the melting point to a higher value. However, the melting temperatures of iron and vanadium measured by recent dynamic experiments[1,71] are overall consistent with the results obtained by both laser-heated DAC experiments and theoretical calculations,[3–5,37,68,71] indicating that the discrepancies are mainly due to the experimental techniques in the previous dynamic experiments. Some experiments and theories found that the relaxation times of electron–electron, electron–phonon, and phonon–phonon thermalization in metals after lattice excitations are lesser than a picosecond (10^{-12} s).[72–74] The fast relaxation time indicates that the

equilibrium will be established very quickly in shocked metals, supporting that there is no remarkable superheating effect of metals in dynamic or static compression experiments.[1,26,71,75,76] Thus, we did not consider the shock-induced superheating in this study.

The Fe–11Ni–18Cr alloy was shocked or released into a mixed-phase where the solid and liquid phases coexist. Thus, in the solid–liquid mixed-phase region, the melting temperature (T_M) at the Hugoniot state can be obtained because T_M is equal to T_H for partial melting.[77] Based on a heat conduction model, the T_M of the mixed-phase at P_R can be obtained from the shock-induced initial melting and subsequent solidification.[53,78–80] When the Fe–11Ni–18Cr alloy was partially released to P_R, it remained in the mixed-phase.[81] The temperature of the window (T_W) is significantly lower than that of the mixed-phase (T_R), resulting in a thermal conduction between the Fe–11Ni–18Cr alloy and the LiF window. The thermal conduction would result in a subsequent solidification of the mixed-phase at the measured interface temperature (T_I) and P_R. Therefore, the T_M at P_R can be constrained by solving the heat conduction equations at the conditions of the boundary between the sample and window, as described in detail elsewhere.[1,78,79] According to the temperature distribution across the interface between the sample and window in Tan–Ahrens' model, T_M was constrained between T_I and T_R at P_R,[79]

$$T_M = T_I - [(T_I - T_W)erf(\mu)]/\alpha, \quad (5)$$

where $erf(\mu)$ is the error function related to the heat diffusivity of the sample, which is approximately equal to −0.5.[53] Therefore, the T_M value is approximated to the median from T_I to T_R,[53]

$$T_M \cong T_I + (T_I - T_W)/(2\alpha) = (T_I + T_R)/2. \quad (6)$$

The semiempirical Simon–Glatzel equation[82] can be used to fit the melting curve over a large range of high pressures for a variety of metals[68,75,83–99] and alloys,[15,34,35,100–104]

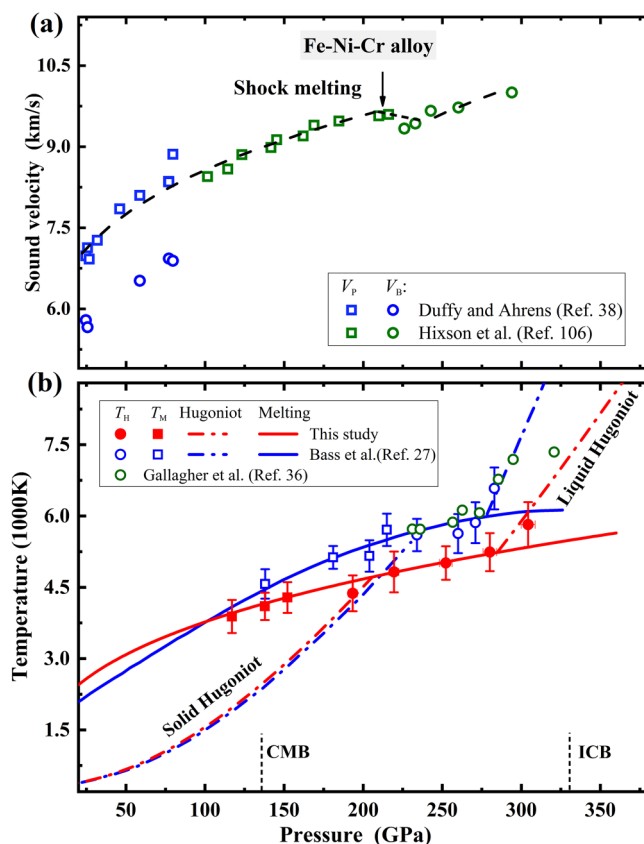$$T_M = T_0\left(\frac{P - P_0}{a} + 1\right)^{\frac{1}{b}}, \quad (7)$$

FIG. 5. Experimental data on the shock melting of the Fe–Ni–Cr alloy at high pressures. (a) Sound velocities of the Fe–Ni–Cr alloy at high pressures. Open squares and open circles are the compressional and bulk sound velocities of the Fe–Ni–Cr alloy, respectively;[38,106] and the sound-velocity discontinuity occurs at a pressure of ∼210 GPa, indicating that the Fe–Ni–Cr alloy starts to melt under shock loading. (b) Measured temperatures of the Fe–Ni–Cr alloy along the Hugoniot curve and partially released states under shock loading and a comparison with previous measurements. Solid red squares and circles represent our determined melting temperatures and Hugoniot temperatures of the Fe–11Ni–18Cr alloy, respectively; open blue squares,[27] open blue circles,[27] and open green circles[36] represent the previously measured melting temperatures and Hugoniot temperatures of the Fe–9Ni–19Cr films, respectively; solid red and blue lines represent the fitted melting curves of the Fe–Ni–Cr alloys in this study and Ref. 27, respectively; and red and blue dashed-dotted lines represent the calculated Hugoniot temperatures of the Fe–Ni–Cr alloy in this study and Ref. 27, respectively. CMB, core-mantle boundary and ICB, inner-core boundary.

where a and b are fitting parameters, T_M and P are the thermodynamic conditions of the melting curve, and T_0 and P_0 are the coordinates of the starting point of the melting curve. The melting curve of the Fe–11Ni–18Cr alloy was obtained by fitting the determined melting temperatures at P_R and P_H from 119 to 280 GPa to the Simon–Glatzel equation (Fig. 5). The obtained fitting parameters are $a = 10$ (2) and $b = 3.01$ (0.15) when taking the starting melting point $T_0 = 1700$ K at a reference pressure $P_0 = 0$ GPa.[105]

Consequently, we obtained the P–T curve of the liquid Fe–11Ni–18Cr along the Hugoniot from the solid Hugoniot by subtracting a temperature change (ΔT) due to the latent heat of melting ($\Delta T = T_{om}\Delta S/C_V$, T_{om}, and ΔS are the temperatures at which the melting starts and the entropy change of melting, respectively)[42] (Fig. 5). Our determined solid and liquid Hugoniot curves showed a discontinuity between ∼210 (8) GPa [4700 (300) K] and ∼280 (10) GPa [5250 (350) K], indicating a complete molten Fe–11Ni–18Cr above ∼280 GPa under shock loading. Meanwhile, the measured sound velocity of the Fe–Ni–Cr alloy shows that the shocked sample starts to melt along the Hugoniot at ∼210 GPa and completely melts at ∼245 GPa (Fig. 5).[106] The onset of melting for the Fe–Ni–Cr alloy determined from the temperature measurement agrees well with the estimated value from the sound-velocity measurements, while the completing pressure is ∼35 GPa higher. Therefore, further reliable experiments are required to measure the sound velocity along the Hugoniot curve in order to accurately determine its melting behaviors.

Based on the fitted melting curve, the melting temperatures of the Fe–11Ni–18Cr alloy are constrained to be 4100 (250) and 5500 (450) K at 136 and 330 GPa, respectively. Compared to the literature values,[27] our determined melting temperature of the Fe–Ni–Cr alloy is ∼700 K lower than the previous estimates at near ICB pressure (Fig. 5).

IV. GEOPHYSICAL IMPLICATIONS

A. Temperature at the inner-core boundary (T_{ICB})

The obtained melting curve of the Fe–11Ni–18Cr alloy is compared with the melting curves of Fe,[1] Ni,[87] and other Fe alloys[13,42] at the outer core pressures (Fig. 6). The melting temperature of the Fe–11Ni–18Cr alloy is lower than that of Fe under high pressures. Considering the uncertainties of the melting temperatures, the real differences in the melting temperature among these metals and alloys are difficult to highlight at the ICB pressure.[107] However, we can estimate the effects of Ni and Cr on the melting temperature of Fe at the ICB pressure, as previous studies did.[12,42,87] The melting curve of pure Ni[86,87] is close to that of Fe, which is only ∼200 K lower than that of Fe at the ICB pressure.[1] Assuming a linear relationship between the two end-members,[87,108] the melting temperature depression in Fe is estimated to be ∼1.5 K/wt. % for Ni. Similarly, we estimate a decrease of ∼25 K/wt. % Cr in the melting temperature of Fe. Compared with the effects of the candidate light elements (such as Si, O, or S) on the melting temperature of Fe,[12,13,42] our result suggests that the addition of a small amount of Ni and Cr has a minor depression effect on the melting temperature of Fe at the ICB pressure.

Based on geochemical, cosmochemical, and meteorite compositional evidence, it is suggested that the Earth's core contains approximately 5–10 wt. % Ni and ∼1 wt. % Cr.[11] Consequently, the alloying of Ni and Cr may decrease the melting temperature of Fe by ∼33–40 K at the ICB pressure. For some model core compositions including 5–10 wt. % light elements,[109,110] we suggest a reasonable value of ∼5400–5600 K at the ICB using less extrapolative estimation taking into account the effects of Ni, Cr, and light elements on the melting point of Fe.
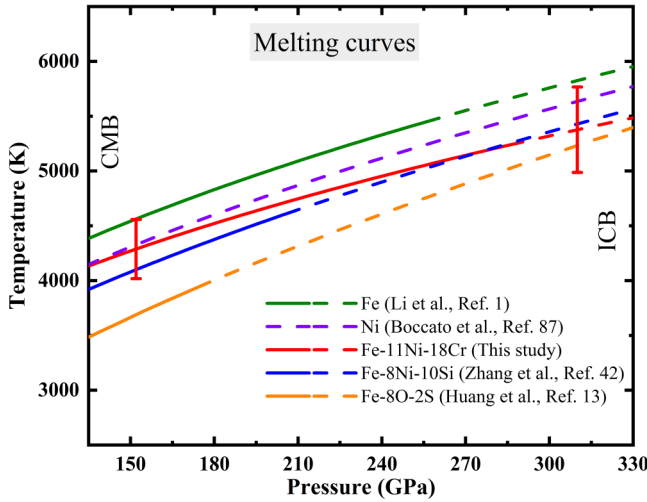
FIG. 6. Melting curve of the Fe–11Ni–18Cr alloy and comparison with the melting curves of Ni, Fe, and Fe alloys with candidate light elements at the outer core pressures. Solid and dashed green lines represent the experimental and extrapolated melting curve of Fe;[1] violet dashed line represents the extrapolated melting curve of Ni;[87] solid and dashed red lines represent the experimental and extrapolated melting curve of the Fe–11Ni–18Cr alloy in this study; solid and dashed blue lines represent the experimental and extrapolated melting curve of the Fe–8Ni–10Si alloy;[42] and solid and dashed yellow lines represent the experimental and extrapolated melting curve of Fe–8O–2S.[13] Red vertical ticks represent the error bars for the melting curve of the Fe–11Ni–18Cr alloy.

FIG. 7. Pressure–density profiles of Fe, Ni, and Fe–Ni alloys at high pressures and compared with seismological observations. Open red, orange, and blue circles represent the shock Hugoniot data of Fe,[23] Ni,[24] and Fe–11Ni–18Cr,[24] respectively; open carmine, green, and dark yellow diamonds represent the shock Hugoniot data of Fe–Ni alloys containing 10, 17.9, and 26.2 wt. % Ni, respectively;[24] black asterisks represent the density of seismic observations from the Preliminary Reference Earth Model (PREM);[111] solid red, orange, and blue lines represent the solid Hugoniot of Fe,[23] Ni,[24] and Fe–11Ni–18Cr,[24] respectively; dashed red and blue lines represent the liquid Hugoniot of Fe[23] and Fe–11Ni–18Cr,[24] respectively; and violet crosses represent the calculated isothermal P–ρ of liquid Fe–11Ni–18Cr up to the ICB pressure at 5500 K. The upper limit of the core density deficit (cdd) is estimated to be ~9.4% at the ICB based on the calculated density of liquid Fe–11Ni–18Cr.

B. Density of liquid Fe–11Ni–18Cr at relevant conditions of the Earth's outer core

To evaluate the effects of Ni and Cr on the density of the outer core,[111] the P–ρ profiles of Fe–11Ni–18Cr and Fe–(10–26.2)Ni alloys are compared with that of pure Fe and Ni along the principal Hugoniot (Fig. 7).[23,24] The Hugoniot density of solid pure Ni is larger than that of solid pure Fe,[23,24] while the addition of 5–18 wt. % Ni into Fe does not significantly change its density under high P–T conditions in DAC experiments[18,112–114] and shock compression experiments (Fig. 7).[23,24] It is noteworthy that the Hugoniot density of solid Fe (or Fe–Ni) is slightly reduced with the addition of 18 wt. % Cr at high P–T. With the increase of shock pressure, the density difference between Fe–11Ni–18Cr and Fe becomes narrow and even indistinguishable after shock-induced melting.[23,24] Because the shock temperature of the Fe–11Ni–18Cr is slightly lower than that of pure Fe, alloying a certain amount of Ni and Cr does not modify the density of Fe in the liquid state at the outer core conditions.

The determined P–T–ρ of liquid Fe–11Ni–18Cr allows us to establish its thermal EoS and estimate the upper limit of the cdd in the outer core. Thermal EoS of liquid Fe–11Ni–18Cr was obtained using a single EoS model based on the Mie–Grüneisen equation,[115]

$$P(V, T) = P_{T_0}(V) + \Delta P_{th}(V, T), \tag{8}$$

where $P(V, T)$ is the total pressure, which is the sum of the pressures at a reference temperature $P_{T_0}(V)$ and a thermal pressure $\Delta P_{th}(V, T)$
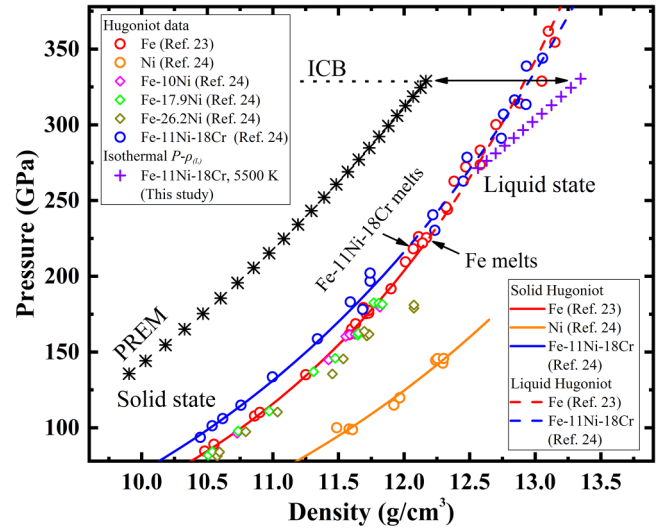
and T_0 is a reference temperature of 1700 K taken from the melting point of Fe–11Ni–18Cr alloy at ambient pressure. $P_{T_0}(V)$ can be calculated by the Vinet (Morse–Rydberg) equation,[116]

$$P_{T_0}(V) = 3K_{T_0} \left(\frac{V}{V_0}\right)^{\frac{-2}{3}} \left[1 - \left(\frac{V}{V_0}\right)^{\frac{1}{3}}\right] \exp\left\{\frac{3}{2}(K'_{T_0} - 1)\left[1 - \left(\frac{V}{V_0}\right)^{\frac{1}{3}}\right]\right\}, \tag{9}$$

where K_{T_0} and K'_{T_0} are the isothermal bulk modulus and its pressure derivative at zero pressure and T_0, respectively. $\Delta P_{th}(V, T)$ can be expressed as follows:[115]

$$\Delta P_{th}(V, T) = \frac{\gamma(V)}{V}\Delta E_{th}(V, T) = \frac{\gamma(V)}{V}[E_{th}(V, T) - E_{th}(V, T_0)], \tag{10}$$

where $\gamma(V)$ is the Grüneisen parameter and $E_{th}(V, T)$ is the internal thermal energy. The volume dependence of $\gamma(V)$ can be considered as[21]

$$\gamma(V) = \gamma_0 \left(\frac{V}{V_0}\right)^b . \qquad (11)$$

The internal thermal energy $[E_{th}(V, T)]$ could be simply represented by a second-order polynomial of temperature with a volume-dependent second-order coefficient as follows:[115]

$$E_{th}(V, T) = 3nR\left(T + e_0 \left(\frac{V}{V_0}\right)^g T^2\right), \qquad (12)$$

where n is the number of atoms in the formula unit; R is the gas constant; and e_0 and g are constants. The EoS parameters of liquid Fe–11Ni–18Cr were determined by combining our shock temperature measurements with previous shock Hugoniot data,[24] where the EoS parameters were as follows: $T_0 = 1700$ K,[105] $\rho_0 = 7.06$ g/cm^3,[117] $K_{T_0} = 92$ GPa, $K'_{T_0} = 5.2$, $\gamma_0 = 2.2$, $b = 0.7$, $e_0 = 0.68 \times 10^{-4}$ K^{-1}, and $g = -1$. We then obtained isothermal P–T–ρ data for the liquid Fe–18Cr–11Ni at 5500 K (the melting temperature of Fe–11Ni–18Cr at the ICB pressure). Thus, the upper limit of the cdd is estimated to be ~9.4 % at the ICB. Our study suggests that sufficient light elements are required in the outer core to satisfy the cdd.

V. CONCLUSIONS

The shock temperatures of an Fe–11Ni–18Cr alloy are determined up to ~304 GPa and ~5820 K using a time-resolved quasi-spectral optical pyrometer in a two-stage light-gas gun. The melting curve of the Fe–11Ni–18Cr alloy is determined up to ~280 GPa. The melting temperatures of the Fe–11Ni–18Cr alloy at CMB and ICB are constrained to be approximately 4100 (250) and 5500 (450) K, respectively, which are slightly lower than that of pure iron. Our study indicates that the integration of limited amounts of Ni and Cr into iron has a minor effect on its melting behavior and liquid density, suggesting that a significant amount of light elements are required in the outer core.

AUTHOR DECLARATIONS
Conflict of Interest

The authors declare no conflict of interest.

DATA AVAILABILITY

The data that support the findings of this study are available from the corresponding authors upon reasonable request.

REFERENCES

[1]J. Li, Q. Wu, J. Li, T. Xue, Y. Tan et al., "Shock melting curve of iron: A consensus on the temperature at the Earth's inner core boundary," Geophys. Res. Lett. 47, e2020GL087758, https://doi.org/10.1029/2020GL087758 (2020).

[2]D. Alfè, "Temperature of the inner-core boundary of the Earth: Melting of iron at high pressure from first-principles coexistence simulations," Phys. Rev. B 79, 060601(R) (2009).

[3]D. Alfè, G. D. Price, and M. J. Gillan, "Iron under Earth's core conditions: Liquid-state thermodynamics and high-pressure melting curve from ab initio calculations," Phys. Rev. B 65, 165118 (2002).

[4]S. Anzellini, A. Dewaele, M. Mezouar, P. Loubeyre, and G. Morard, "Melting of iron at Earth's inner core boundary based on fast x-ray diffraction," Science 340, 464 (2013).

[5]G. Morard, S. Boccato, A. D. Rosa, S. Anzellini, F. Miozzi et al., "Solving controversies on the iron phase diagram under high pressure," Geophys. Res. Lett. 45, 11074, https://doi.org/2018GL079950 (2018).

[6]S. J. Turneaure, S. M. Sharma, and Y. M. Gupta, "Crystal structure and melting of Fe shock compressed to 273 GPa: In situ x-ray diffraction," Phys. Rev. Lett. 125, 215702 (2020).

[7]M. Hou, J. Liu, Y. Zhang, X. Du, H. Dong et al., "Melting of iron explored by electrical resistance jump up to 135 GPa," Geophys. Res. Lett. 48, e2021GL095739, https://doi.org/10.1029/2021GL095739 (2021).

[8]R. Sinmyo, K. Hirose, and Y. Ohishi, "Melting curve of iron to 290 GPa determined in a resistance-heated diamond-anvil cell," Earth Planet. Sci. Lett. 510, 45 (2019).

[9]B. Gan, J. Li, G. Jiang, and Y. Zhang, "A review of the experimental determination of the melting curve of iron at ultrahigh pressures," Chin. J. High Pressure Phys. 35, 060101 (2021).

[10]J. Li and Y. Fei, "Experimental constraints on core composition," in Treatise on Geochemistry, 2nd ed., edited by H. D. Holland and K. K. Turekian (Oxford Elsevier, 2014), p. 527.

[11]W. F. McDonough, "Compositional model for the Earth's core," in Treatise on Geochemistry, 2nd ed., edited by H. D. Holland and K. K. Turekian (Oxford Elsevier, 2014), p. 559.

[12]R. A. Fischer, "Melting of Fe alloys and the thermal structure of the core," in Deep Earth Physics and Chemistry of the Lower Mantle and Core, edited by H. Terasaki and R. A. Fischer (John Wiley, Hoboken, 2016), p. 3.

[13]H. Huang, X. Hu, F. Jing, L. Cai, Q. Shen et al., "Melting behavior of Fe-O-S at high pressure: A discussion on the melting depression induced by O and S," J. Geophys. Res. 115, B05207, https://doi.org/10.1029/2009JB006514 (2010).

[14]Y. Fei and C. Bertka, "The interior of Mars," Science 308, 1120 (2005).

[15]H. Terasaki, S. Kamada, T. Sakai, E. Ohtani, N. Hirao et al., "Liquidus and solidus temperatures of a Fe–O–S alloy up to the pressures of the outer core: Implication for the thermal structure of the Earth's core," Earth Planet. Sci. Lett. 304, 559 (2011).

[16]Z. Zou, K. D. Koper, and V. F. Cormier, "The structure of the base of the outer core inferred from seismic waves diffracted around the inner core," J. Geophys. Res. Solid Earth 113, B05314, https://doi.org/10.1029/2007JB005316 (2008).

[17]H. Huang, Y. Fei, L. Cai, F. Jing, X. Hu et al., "Evidence for an oxygen-depleted liquid outer core of the Earth," Nature 479, 513 (2011).

[18]O. L. Anderson and D. G. Isaak, "Another look at the core density deficit of Earth's outer core," Phys. Earth Planet. Inter. 131, 19 (2002).

[19]J.-P. Poirier, "Light elements in the Earth's outer core: A critical review," Phys. Earth Planet. Inter. 85, 319 (1994).

[20]H.-K. Mao, B. Chen, J. Chen, K. Li, J.-F. Lin et al., "Recent advances in high-pressure science and technology," Matter Radiat. Extremes 1, 59 (2016).

[21]Y. Kuwayama, G. Morard, Y. Nakajima, K. Hirose, A. Q. R. Baron et al., "Equation of state of liquid iron under extreme conditions," Phys. Rev. Lett. 124, 165701 (2020).

[22]J. M. Brown and R. G. McQueen, "Phase transitions, Grüneisen parameter, and elasticity for shocked iron between 77 GPa and 400 GPa," J. Geophys. Res. Solid Earth 91, 7485, https://doi.org/10.1029/JB091iB07p07485 (1986).

[23]J. M. Brown, J. N. Fritz, and R. S. Hixson, "Hugoniot data for iron," J. Appl. Phys. 88, 5496 (2000).

[24]S. P. Marsh, LASL Shock Hugoniot Data (University of California Press, Berkeley, 1980).

[25]Q. Williams, R. Jeanloz, J. Bass, B. Svendsen, and T. J. Ahrens, "The melting curve of iron to 250 gigapascals: A constraint on the temperature at Earth's center," Science 236, 181 (1987).

[26]C. S. Yoo, N. C. Holmes, M. Ross, D. J. Webb, and C. Pike, "Shock temperatures and melting of iron at Earth core conditions," Phys. Rev. Lett. 70, 3931, (1993).

[27]J. D. Bass, T. J. Ahrens, J. R. Abelson, and T. Hua, "Shock temperature measurements in metals: New results for an Fe alloy," J. Geophys. Res. 95, 21767, https://doi.org/JB095iB13p21767 (1990).

[28]C. K. Gessmann and D. C. Rubie, "The origin of the depletions of V, Cr and Mn in the mantles of the Earth and Moon," Earth Planet. Sci. Lett. 184, 95 (2000).

[29]F. Moynier, Q.-Z. Yin, and E. Schauble, "Isotopic evidence of Cr partitioning into Earth's core," Science 331, 1417 (2011).

[30]H. Palme and H. S. C. O'Neill, "Cosmochemical estimates of mantle composition," in Treatise on Geochemistry, edited by H. D. Holland and K. K. Turekian (Elsevier-Pergamon, Oxford, 2003), Vol. 2, p. 1.

[31]J. Wade and B. J. Wood, "Core formation and the oxidation state of the Earth," Earth Planet. Sci. Lett. 236, 78 (2005).

[32]B. J. Wood, J. Wade, and M. R. Kilburn, "Core formation and the oxidation state of the Earth: Additional constraints from Nb, V and Cr partitioning," Geochim. Cosmochim. Acta 72, 1415 (2008).

[33]C. J. Allègre, J.-P. Poirier, E. Humler, and A. W. Hofmann, "The chemical composition of the Earth," Earth Planet. Sci. Lett. 134, 515 (1995).

[34]R. Torchio, S. Boccato, F. Miozzi, A. D. Rosa, N. Ishimatsu et al., "Melting curve and phase relations of Fe-Ni alloys: Implications for the Earth's core composition," Geophys. Res. Lett. 47, e2020GL088169, https://doi.org/10.1029/2020GL088169 (2020).

[35]D. Z. Zhang, J. M. Jackson, J. Zhao, W. Sturhahn, E. E. Alp et al., "Temperature of Earth's core constrained from melting of Fe and Fe$_{0.9}$Ni$_{0.1}$ at high pressures," Earth Planet. Sci. Lett. 447, 72 (2016).

[36]K. G. Gallagher, J. D. Bass, T. J. Ahrens, M. Fitzner, and J. R. Abelson, "Shock temperature of stainless steel and a high pressure—High temperature constraint on thermal diffusity of Al$_2$O$_3$," AIP Conf. Proc. 309, 963 (1994).

[37]T. Sun, J. P. Brodholt, Y. Li, and L. Vočadlo, "Melting properties from ab initio free energy calculations: Iron at the Earth's inner-core boundary," Phys. Rev. B 98, 224301 (2018).

[38]T. S. Duffy and T. J. Ahrens, "Dynamic compression of an Fe-Cr-Ni alloy to 80 GPa," J. Appl. Phys. 82, 4259 (1997).

[39]R. G. McQueen, S. P. Marsh, J. W. Taylor, J. N. Fritz, and W. J. Carter, "The equation of state of solids from shock wave studies," in High-Velocity Impact Phenomena, edited by R. Kinslow (CA Academic Press, San Diego, 1970), p. 293.

[40]W. J. Nellis and C. S. Yoo, "Issues concerning shock temperature measurements or iron and other metals," J. Geophys. Res. 95, 21749, https://dooi.org/10.1029/JB095iB13p21749 (1990).

[41]P. A. Urtiew and R. Grover, "Temperature deposition caused by shock interactions with material interfaces," J. Appl. Phys. 45, 140 (1974).

[42]Y. Zhang, T. Sekine, J.-F. Lin, H. He, F. Liu et al., "Shock compression and melting of an Fe-Ni-Si alloy: Implications for the temperature profile of the Earth's core and the heat flux across the core-mantle boundary," J. Geophys. Res. Solid Earth 123, 1314, https://doi.org/10.1029/2017JB014723 (2018).

[43]P. M. Celliers, G. W. Collins, D. G. Hicks, and J. H. Eggert, "Systematic uncertainties in shock-wave impedance-match analysis and the high-pressure equation of state of Al," J. Appl. Phys. 98, 113529 (2005).

[44]T. J. Ahrens, "6. Shock wave techniques for geophysics and planetary physics," in Methods in Experimental Physics, edited by C. G. Sammis and T. L. Henyey (Academic Press, 1987), Vol. 24, p. 185.

[45]M. H. Rice, R. G. McQueen, and J. M. Walsh, "Compression of solids by strong shock waves," in Solid State Physics, edited by F. Seitz and D. Turnbull (Academic Press, New York, 1958), Vol. 6, p. 1.

[46]A. C. Mitchell and W. J. Nellis, "Shock compression of aluminum, copper, and tantalum," J. Appl. Phys. 52, 3363 (1981).

[47]R. G. Kraus, J.-P. Davis, C. T. Seagle, D. E. Fratanduono, D. C. Swift et al., "Dynamic compression of copper to over 450 GPa: A high-pressure standard," Phys. Rev. B 93, 134105 (2016).

[48]F. Xi, K. Jin, L. Cai, H. Geng, Y. Tan et al., "Sound velocity of tantalum under shock compression in the 18–142 GPa range," J. Appl. Phys. 117, 185901 (2015).

[49]Q. Liu, X. Zhou, X. Zeng, and S. N. Luo, "Sound velocity, equation of state, temperature and melting of LiF single crystals under shock compression," J. Appl. Phys. 117, 045901 (2015).

[50]N. C. Holmes, J. A. Moriarty, G. R. Gathers, and W. J. Nellis, "The equation of state of platinum to 660 GPa (6.6 mbar)," J. Appl. Phys. 66, 2962 (1989).

[51]X. Zhou, W. J. Nellis, J. Li, J. Li, W. Zhao et al., "Optical emission, shock-induced opacity, temperatures, and melting of Gd$_3$Ga$_5$O$_{12}$ single crystals shock-compressed from 41 to 290 GPa," J. Appl. Phys. 118, 055903 (2015).

[52]M. B. Boslough and T. J. Ahrens, "A sensitive time-resolved radiation pyrometer for shock-temperature measurements above 1500 K," Rev. Sci. Instrum. 60, 3711 (1989).

[53]C. Dai, J. Hu, and H. Tan, "Hugoniot temperatures and melting of tantalum under shock compression determined by optical pyrometry," J. Appl. Phys. 106, 043519 (2009).

[54]R. Grover and P. A. Urtiew, "Thermal relaxation at interfaces following shock compression," J. Appl. Phys. 45, 146 (1974).

[55]P. C. Myint, E. L. Shi, S. Hamel, H. Cynn, Z. Jenei et al., "Two-phase equation of state for lithium fluoride," J. Chem. Phys. 150, 074506 (2019).

[56]S. Andersson and G. Backstrom, "Thermal conductivity and heat capacity of single-crystal LiF and CaF2 under hydrostatic pressure," J. Phys. C: Solid State Phys. 20, 5951 (1987).

[57]W.-G. Zhao, X.-M. Zhou, J.-B. Li, J. Li, and X.-L. Zeng, "Thermal conductivity of shocked LiF single crystal measurement by liquid sandwich method," J. At. Mol. Phys. 31, 140 (2014).

[58]R. E. Jones and D. K. Ward, "Estimates of crystalline LiF thermal conductivity at high temperature and pressure by a Green-Kubo method," Phys. Rev. B 94, 014309 (2016).

[59]N. A. Smirnov, "Ab initio calculations of the thermodynamic properties of LiF crystal," Phys. Rev. B 83, 014109 (2011).

[60]J. Xu, P. Zhang, K. Haule, J. Minar, S. Wimmer et al., "Thermal conductivity and electrical resistivity of solid iron at Earth's core conditions from first principles," Phys. Rev. Lett. 121, 096601 (2018).

[61]Y. Zhang, M. Hou, G. Liu, C. Zhang, V. B. Prakapenka et al., "Reconciliation of experiments and theory on transport properties of iron and the geodynamo," Phys. Rev. Lett. 125, 078501 (2020).

[62]Y. Zhang, M. Hou, P. Driscoll, N. P. Salke, J. Liu et al., "Transport properties of Fe-Ni-Si alloys at Earth's core conditions: Insight into the viability of thermal and compositional convection," Earth Planet. Sci. Lett. 553, 116614 (2021).

[63]J. D. Bass, B. Svendsen, and T. J. Ahrens, "The temperature of shock compressed iron," in High-Pressure Research in Mineral Physics: A Volume in Honor of Syun-iti Akimoto, edited by M. H. Manghnani and Y. Syono (Terra Scientific Publishing Company, 1987), Vol. 39, p. 393.

[64]C. Dai, X. Jin, X. Zhou, J. Liu, and J. Hu, "Sound velocity variations and melting of vanadium under shock compression," J. Phys. D: Appl. Phys. 34, 3064 (2001).

[65]D. Errandonea, M. Somayazulu, D. Häusermann, and H. K. Mao, "Melting of tantalum at high pressure determined by angle dispersive x-ray diffraction in a double-sided laser-heated diamond-anvil cell," J. Phys: Condens. Matter 15, 7635 (2003).

[66]D. Errandonea, R. Boehler, and M. Ross, "Melting of the alkaline-earth metals to 80 GPa," Phys. Rev. B 65, 012108 (2001).

[67]A. Dewaele, M. Mezouar, N. Guignot, and P. Loubeyre, "High melting points of tantalum in a laser-heated diamond anvil cell," Phys. Rev. Lett. 104, 255701 (2010).

[68]D. Errandonea, S. G. MacLeod, L. Burakovsky, D. Santamaria-Perez, J. E. Proctor et al., "Melting curve and phase diagram of vanadium under high-pressure and high-temperature conditions," Phys. Rev. B **100**, 094111 (2019).

[69]T. Zhang, S. Wang, H. Song, S. Duan, and H. Liu, "Melting curve of vanadium up to 470 GPa simulated by ab initio molecular dynamics," J. Appl. Phys. **126**, 205901 (2019).

[70]S.-N. Luo and T. J. Ahrens, "Shock-induced superheating and melting curves of geophysically important minerals," Phys. Earth Planet. Inter. **143–144**, 369 (2004).

[71]Y. Zhang, Y. Tan, H. Y. Geng, N. P. Salke, Z. Gao et al., "Melting curve of vanadium up to 256 GPa: Consistency between experiments and theory," Phys. Rev. B **102**, 214104 (2020).

[72]J. Li, Q. Wu, T. Xue, H. Geng, J. Yu et al., "The α-γ-ε triple point and phase boundaries of iron under shock compression," J. Appl. Phys. **122**, 025901 (2017).

[73]J. Siwick Bradley, R. Dwyer Jason, E. Jordan Robert, and R. J. D. Miller, "An atomic-level view of melting using femtosecond electron diffraction," Science **302**, 1382 (2003).

[74]D. C. Wallace, "Irreversible thermodynamics of flow in solids," Phys. Rev. B **22**, 1477 (1980).

[75]R. Boehler and M. Ross, "Melting curve of aluminum in a diamond cell to 0.8 Mbar: Implications for iron," Earth Planet. Sci. Lett. **153**, 223 (1997).

[76]J. H. Nguyen and N. C. Holmes, "Melting of iron at the physical conditions of the Earth's core," Nature **427**, 339 (2004).

[77]C. Dai and H. Tan, "A heat conduction model for three layers and application to shock temperature measurements for metals," J. Phys: Condens. Matter **14**, 10829 (2002).

[78]H. Tan, C. D. Dai, L. Y. Zhang, and C. H. Xu, "Method to determine the melting temperatures of metals under megabar shock pressures," Appl. Phys. Lett. **87**, 221905 (2005).

[79]H. Tan and T. J. Ahrens, "Shock temperature measurements for metals," High Pressure Res. **2**, 159 (1990).

[80]W. W. Anderson and T. J. Ahrens, "Shock temperature and melting in iron sulfides at core pressures," J. Geophys. Res. Solid Earth **101**, 5627, https://doi.org/10.1029/95JB01972 (1996).

[81]B. M. La Lone, G. D. Stevens, W. D. Turley, D. B. Holtkamp, A. J. Iverson et al., "Release path temperatures of shock-compressed tin from dynamic reflectance and radiance measurements," J. Appl. Phys. **114**, 063506 (2013).

[82]F. Simon and G. Glatzel, "Bemerkungen zur Schmelzdruckkurve," Z. Anorg. Allg. Chem. **178**, 309 (1929).

[83]D. Errandonea, "The melting curve of ten metals up to 12 GPa and 1600 K," J. Appl. Phys. **108**, 033517 (2010).

[84]G. Weck, V. Recoules, J.-A. Queyroux, F. Datchi, J. Bouchet et al., "Determination of the melting curve of gold up to 110 GPa," Phys. Rev. B **101**, 014106 (2020).

[85]A. Dewaele, M. Mezouar, N. Guignot, and P. Loubeyre, "Melting of lead under high pressure studied using second-scale time-resolved x-ray diffraction," Phys. Rev. B **76**, 144106 (2007).

[86]O. T. Lord, I. G. Wood, D. P. Dobson, L. Vočadlo, W. Wang et al., "The melting curve of Ni to 1 Mbar," Earth Planet. Sci. Lett. **408**, 226 (2014).

[87]S. Boccato, R. Torchio, I. Kantor, G. Morard, S. Anzellini et al., "The melting curve of nickel up to 100 GPa explored by XAS," J. Geophys. Res. Solid Earth **122**, 9921, https://doi.org/10.1002/2017JB014807 (2017).

[88]F. Cricchio, A. B. Belonoshko, L. Burakovsky, D. L. Preston, and R. Ahuja, "High-pressure melting of lead," Phys. Rev. B **73**, 140103 (2006).

[89]D. Errandonea, "High-pressure melting curves of the transition metals Cu, Ni, Pd, and Pt," Phys. Rev. B **87**, 054108 (2013).

[90]A. B. Belonoshko, L. Burakovsky, S. P. Chen, B. Johansson, A. S. Mikhaylushkin et al., "Molybdenum at high pressure and temperature: Melting from another solid phase," Phys. Rev. Lett. **100**, 135701 (2008).

[91]R. Hrubiak, Y. Meng, and G. Shen, "Microstructures define melting of molybdenum at high pressures," Nat. Commun. **8**, 14562 (2017).

[92]V. Stutzmann, A. Dewaele, J. Bouchet, F. Bottin, and M. Mezouar, "High-pressure melting curve of titanium," Phys. Rev. B **92**, 224110 (2015).

[93]P. Parisiades, F. Cova, and G. Garbarino, "Melting curve of elemental zirconium," Phys. Rev. B **100**, 054102 (2019).

[94]J. S. Pigott, N. Velisavljevic, E. K. Moss, N. Draganic, M. K. Jacobsen et al., "Experimental melting curve of zirconium metal to 37 GPa," J. Phys: Condens. Matter **32**, 355402 (2020).

[95]S. Anzellini, V. Monteseguro, E. Bandiello, A. Dewaele, L. Burakovsky et al., "In situ characterization of the high pressure—High temperature melting curve of platinum," Sci. Rep. **9**, 13034 (2019).

[96]A. B. Belonoshko and A. Rosengren, "High-pressure melting curve of platinum from ab initio Z method," Phys. Rev. B **85**, 174104 (2012).

[97]D. Errandonea, L. Burakovsky, D. L. Preston, S. G. MacLeod, D. Santamaría-Perez et al., "Experimental and theoretical confirmation of an orthorhombic phase transition in niobium at high pressure and temperature," Commun. Mater. **1**, 60 (2020).

[98]L. Burakovsky, N. Burakovsky, and D. L. Preston, "Ab initio melting curve of osmium," Phys. Rev. B **92**, 174105 (2015).

[99]N. N. Patel and M. Sunder, "High pressure melting curve of osmium up to 35 GPa," J. Appl. Phys. **125**, 055902 (2019).

[100]G. Morard, D. Andrault, N. Guignot, J. Siebert, G. Garbarino et al., "Melting of Fe–Ni–Si and Fe–Ni–S alloys at megabar pressures: Implications for the core–mantle boundary temperature," Phys. Chem. Miner. **38**, 767 (2011).

[101]H. Asanuma, E. Ohtani, T. Sakai, H. Terasaki, S. Kamada et al., "Melting of iron–silicon alloy up to the core–mantle boundary pressure: Implications to the thermal structure of the Earth's core," Phys. Chem. Miner. **37**, 353 (2010).

[102]R. A. Fischer, A. J. Campbell, D. M. Reaman, N. A. Miller, D. L. Heinz et al., "Phase relations in the Fe–FeSi system at high pressures and temperatures," Earth Planet. Sci. Lett. **373**, 54 (2013).

[103]S. Kamada, E. Ohtani, H. Terasaki, T. Sakai, M. Miyahara et al., "Melting relationships in the Fe–Fe3S system up to the outer core conditions," Earth Planet. Sci. Lett. **359–360**, 26 (2012).

[104]O. T. Lord, M. J. Walter, R. Dasgupta, D. Walker, and S. M. Clark, "Melting in the Fe–C system to 70 GPa," Earth Planet. Sci. Lett. **284**, 157 (2009).

[105]J. R. Lewis, "Physical properties of stainless steels," in Handbook of Stainless Steels, edited by D. Peckher and I. M. Bernstein (McGraw-Hill, New York, 1977), Vol. 19, p. 1.

[106]R. S. Hixson, R. G. McQueen, and J. N. Fritz, "The shock Hugoniot of 316 SS and sound velocity measurements," AIP Conf. Proc. **309**, 105 (1994).

[107]J. R. Taylor, in Introduction to Error Analysis, the Study of Uncertainties in Physical Measurements, 2nd ed. (University Science Books, 1997).

[108]Y. Kuwayama, K. Hirose, N. Sata, and Y. Ohishi, "Phase relations of iron and iron-nickel alloys up to 300 GPa: Implications for composition and structure of the Earth's inner core," Earth Planet. Sci. Lett. **273**, 379 (2008).

[109]K. Hirose, S. Labrosse, and J. Hernlund, "Composition and state of the core," Annu. Rev. Earth Planet. Sci. **41**, 657 (2013).

[110]Y. Zhang, T. Sekine, H. He, Y. Yu, F. Liu et al., "Experimental constraints on light elements in the Earth's outer core," Sci. Rep. **6**, 22473 (2016).

[111]A. M. Dziewonski and D. L. Anderson, "Preliminary reference Earth model," Phys. Earth Planet. Inter. **25**, 297 (1981).

[112]A. P. Kantor, I. Yu. Kantor, A. V. Kurnosov, A. Yu. Kuznetsov, N. A. Dubrovinskaia et al., "Sound wave velocities of fcc Fe–Ni alloy at high pressure and temperature by mean of inelastic x-ray scattering," Phys. Earth Planet. Inter. **164**, 83 (2007).

[113]J. Shanker, B. P. Singh, and S. K. Srivastava, "Volume–temperature relationship for iron at 330 GPa and the Earth's core density deficit," Phys. Earth Planet. Inter. **147**, 333 (2004).

[114]R. A. Morrison, J. M. Jackson, W. Sturhahn, D. Zhang, and E. Greenberg, "Equations of state and anisotropy of Fe-Ni-Si alloys," J. Geophys. Res. Solid Earth **123**, 4647, https://doi.org/10.1029/2017JB015343 (2018).

[115]H. Ichikawa, T. Tsuchiya, and Y. Tange, "The P-V-T equation of state and thermodynamic properties of liquid iron," J. Geophys. Res. Solid Earth **119**, 240, https://doi.org/10.2013JB010732 (2014).

[116]F. D. Stacey and P. M. Davis, "High pressure equations of state with applications to the lower mantle and core," Phys. Earth Planet. Inter. **142**, 137 (2004).

[117]T. Matsumoto, T. Misono, H. Fujii, and K. Nogi, "Surface tension of molten stainless steels under plasma conditions," J. Mater. Sci. **40**, 2197 (2005).